



# *Bacillus thuringiensis* toxin Cyt2Aa forms filamentous oligomers when exposed to lipid membranes or detergents



Gašper Šolinc <sup>a, b</sup>, Gregor Anderluh <sup>a</sup>, Marjetka Podobnik <sup>a, \*</sup>

<sup>a</sup> Department of Molecular Biology and Nanobiotechnology, National Institute of Chemistry, Hajdrihova ulica 19, 1000, Ljubljana, Slovenia

<sup>b</sup> Biotechnical Faculty, University of Ljubljana, Jamnikarjeva ulica 101, 1000, Ljubljana, Slovenia

## ARTICLE INFO

### Article history:

Received 26 May 2023

Received in revised form

6 June 2023

Accepted 25 June 2023

Available online 26 June 2023

### Keywords:

*Bacillus thuringiensis*

Parasporal crystal delta-endotoxins

Cyt toxin

Cyt2Aa

Oligomers

Detergent-like mechanism of action

## ABSTRACT

The bacterium *Bacillus thuringiensis* (*Bt*) produces insecticidal proteins during the sporulation phase. These proteins are located in parasporal crystals consisting of two delta-endotoxin classes, crystal (Cry) and cytolytic (Cyt) toxins. *In vitro*, Cyt toxins show cytolytic activity against bacterial and a variety of insect and mammalian cells. They bind to cell membranes with unsaturated phospholipids and sphingomyelin. Although *Bt* and its parasporal crystals containing both Cry and Cyt toxins have been successfully used as bioinsecticides, the molecular mechanism of action of Cyt toxins is not yet fully understood. To address this, we exposed Cyt2Aa to lipid membranes and visualized membrane disruption process using cryo-electron microscopy. We observed two types of Cyt2Aa oligomers. First, Cyt2Aa forms smaller curved oligomers on the membrane surface that become linear over time, and detach when the membrane ruptures. Similar linear filamentous oligomers were also formed by Cyt2Aa in the presence of detergents without prior exposure to lipid membranes, which exhibited attenuated cytolytic activity. Furthermore, our data suggest that Cyt2Aa adopts different conformations between its monomeric and oligomeric forms. Overall, our results provide new evidence for a detergent-like mechanism of action of Cyt2Aa rather than the pore-forming model of target membrane disruption of this important class of insecticidal proteins.

© 2023 The Authors. Published by Elsevier Inc. This is an open access article under the CC BY-NC-ND license (<http://creativecommons.org/licenses/by-nc-nd/4.0/>).

## 1. Introduction

*Bacillus thuringiensis* (*Bt*) is successfully used as a pesticide worldwide [1,2]. The important source of insecticidal activity are its parasporal crystals formed during sporulation [3]. These parasporal crystals contain insecticidal proteins that have been classified into two delta-endotoxin classes of crystal (Cry) and cytolytic (Cyt) toxins [4,5]. The Cry proteins form a large class with over 750 members, and are three-domain toxins with a size of about 60 kDa that require a protein receptor to bind target membranes and form pores [6,7]. In contrast, Cyt toxins form a comparatively smaller class of 20 kDa proteins with around 40 members [7,8] that do not require a specific receptor for membrane binding and subsequent lysis [9]. Although they differ at the structural level, both groups of toxins exhibit larvicidal activity [10,11]. During sporulation, Cyt toxins are produced along with other insecticidal proteins, and

synergistic interactions between Cyt and Cry toxins have been described previously [6,12–15]. In some cases, the presence of Cyt toxins in *Bt* crystals has helped overcome Cry toxin resistance in insects [6,16–18]. In addition, strong interactions between Cyt and Cry proteins indicated that Cyt may function as a receptor for Cry proteins [15,19]. Thus, the expression of Cyt/Cyt toxins and other insecticidal proteins has made *Bt* the most successful bioinsecticide [1,20].

Cyt toxins have been classified into 8 primary subclasses Cyt1–Cyt8 based on their amino acid identity [5,8]. Cyt2Aa was originally discovered in *Bt* subsp. *kyushuensis* [21] and later characterized as a 259 amino acid long pro-toxin [22]. The three-dimensional structures of the Cyt toxins, including the protoxin form of Cyt2Aa protoxin (previously named CytB; UniProt-Q04470) [8,10], Cyt1Aa protoxin [23] and the activated form of Cyt2Ba [24] and Cyt1Aa [25] are highly conserved, suggesting a similar mechanism of action. Activation of Cyt toxins occurs in the insect midgut, where approximately 30 amino acid residues are removed by proteolysis from both the N- and C-termini of the protein [26,27]. *In vitro*, Cyt toxins exhibit cytolytic activity against bacterial cells [28] and a

\* Corresponding author.

E-mail addresses: [gasper.solinc@ki.si](mailto:gasper.solinc@ki.si) (G. Šolinc), [gregor.anderluh@ki.si](mailto:gregor.anderluh@ki.si) (G. Anderluh), [marjetka.podobnik@ki.si](mailto:marjetka.podobnik@ki.si) (M. Podobnik).

**Abbreviations**

CHOL	(cholesterol)
cryo-EM	(cryogenic electron microscopy)
DDM	(n-dodecyl $\beta$ -D-maltoside)
DOPC	(1,2-dioleoyl- <i>sn</i> -glycero-3-phosphocholine)
DPhPC	(1,2-diphytanoyl- <i>sn</i> -glycero-3-phosphocholine)
Fos-Choline-12 (FC-12)	
Fos-Choline-16 (FC-16)	
LUV	(large unilamellar vesicle)
MLV	(multilamellar vesicle)
PDB	(Protein Data Bank)
POPC	(1-palmitoyl-2-oleoyl-glycero-3-phosphocholine)
POPG	(1-palmitoyl-2-oleoyl- <i>sn</i> -glycero-3-phospho-(1'-rac-glycerol))
RBC	(bovine red blood cell)
SM	(sphingomyelin)
TX-100	(Triton X-100)

variety of insect and mammalian cells [9,29,30], while *in vivo* they display Diptera-specific toxicity [21,31,32].

Cyt toxins bind to membranes composed of unsaturated lipids [9,33]. Cyt1Aa [23,34] and Cyt2Aa [35] form detergent-resistant oligomers when exposed to lipid membranes, which could be visualized by SDS-PAGE analysis. These oligomers were of heterogeneous size and appeared as a ladder-like pattern (or smear) on the gel. Experiments with planar lipid bilayers suggested that Cyt1Aa [36] and Cyt2Aa [21] form cation-selective channels or pores in the membrane. Several studies on Cyt toxins [21,29,36–38] suggested that lysis of the target membrane by these toxins could occur through the formation of well-defined oligomeric transmembrane pores, supporting the pore-forming model [39]. On the other hand, several other studies [9,23,40–44] suggested that Cyt might act via a detergent-like mechanism of action [45], in which Cyt aggregates on the surface of the lipid membrane and consequently forms nonspecific defects in the lipid bilayer. However, the details at the molecular level that would ultimately explain the mechanism of membrane disruption by Cyt toxins, remain to be determined.

Given the importance of *Bt* in general and its crystal toxins in particular as bioinsecticides, it is important to understand the mechanism of target membrane disruption by these toxins at the molecular level. In this work, we investigated the mechanism of action of a Cyt toxin by studying the interaction of recombinant *Bt* Cyt2Aa with lipid membranes, the oligomerization process, and the structure of Cyt2Aa oligomers. We discovered two types of oligomers with cryo-EM, possibly representing two different steps in the membrane disruption process. Our results suggest that the mechanism of membrane disruption of Cyt2Aa does not involve ring-shaped transmembrane pores, but that membranes are ruptured by a detergent-like mechanism.

## 2. Material and methods

### 2.1. Protein expression and purification

The gene encoding Cyt2Aa in a protoxin form (UniProt-Q04470) was cloned into a modified pET24a vector. The recombinant protein was produced in *E. coli* BL21 (DE3). Bacterial cultures were grown in 1 l of Terrific Broth medium containing 100  $\mu$ g/ml ampicillin at 37 °C with constant shaking. When culture absorbance at 600 nm reached 0.6–0.8, protein expression was induced by the addition of

0.4 mM isopropyl 1-thio- $\beta$ -D-galactopyranoside. After overnight incubation at 20 °C, cells were harvested by 5 min centrifugation at 4 °C and 6000 $\times$ g, and re-suspended in 50 ml of the phosphate buffer saline (PBS) in 150 mM NaCl, 20 mM DTT, 50 mM carbonate buffer (Na<sub>2</sub>CO<sub>3</sub>:NaHCO<sub>3</sub> 4:1, mol:mol), pH 10.5 and sonicated. Cell lysate was centrifuged at 50,000 $\times$ g, 4 °C for 45 min and at 68,000 $\times$ g for 5 min. The supernatant was filtered using a 0.22  $\mu$ m syringe filter (TPP, Switzerland) and loaded onto a StrepTrap HP 5 ml column (GE Healthcare, UK) and proteins were eluted with six column volumes of elution buffer with 2.5 mM desthiobiotin (Sigma-Aldrich, USA). Protoxin containing fractions were pulled. Protein concentration was estimated with Nanodrop One (Thermo Fisher Scientific, USA). The protoxin was activated by incubating the protein with 1% (w/w) proteinase K (Thermo Fisher Scientific, USA) for 1 h at 37 °C. Proteinase was inhibited with cOmplete™ Protease Inhibitor Cocktail (Roche, Switzerland). Activation was followed by gel filtration on 320 ml Superdex 200 column (GE Healthcare, UK) with PBS (1.8 mM KH<sub>2</sub>PO<sub>4</sub>, 140 mM NaCl, 10.1 mM NaHPO<sub>4</sub>, 2.7 mM KCl, pH 7.4) to further separate Cyt2Aa from the protease and other impurities (Fig. 1 A). The purified Cyt2Aa was concentrated, aliquoted and stored at –20 °C.

### 2.2. Thermal stability assay

The thermal stability of Cyt2Aa was investigated with a differential scanning fluorimetry assay using 2x SYPRO Orange dye (Thermo Fisher Scientific, USA). The protein concentration used was 0.1 mg/ml. Thermal stability of proteins was tested at 150 mM NaCl and 10 mM SPG buffer (succinic acid, sodium dihydrogen phosphate, and glycine in the molar ratios 2:7:7) at indicated pH values. The protein solution was exposed to a temperature range spanning from 25 °C to 85 °C, with a gradual increase of 1 °C per minute. Thermal stability profiles were recorded using a Light-Cycler 480 (Roche, Switzerland) instrument. To determine the melting temperatures (T<sub>m</sub>), the Boltzmann function was fitted to the curve using Origin 8.1 software (Origin Lab, USA). Each T<sub>m</sub> value represents the average of three separate experiments.

### 2.3. Hemolytic assay

Bovine red blood cells (RBC) were washed, by 3–4 cycles of centrifugation (800 $\times$ g) followed buffer replacement at 21 °C. RBCs were resuspended in buffers containing 140 mM NaCl and 20 mM buffer component, either 2-(N-morpholino)ethanesulfonic acid (MES) pH 5.5, NaH<sub>2</sub>PO<sub>4</sub>/Na<sub>2</sub>HPO<sub>4</sub> pH 6.5, tris(hydroxymethyl)aminomethane (TRIS)/HCl pH 7.4, or glycine pH 8.5 or 9.5. The RBC were resuspended in the appropriate buffer until it reached an absorbance of approximately 0.5 at 630 nm (A<sub>630</sub>) as measured by the Synergy MX microplate reader (Biotek, USA). Subsequently, 100  $\mu$ l of RBC suspension was added to each well of 96-well clear microtiter plate containing 100  $\mu$ l of protein serial dilution (1:1) to reach the final protein concentrations in the range of 1.2 nM–10  $\mu$ M. A<sub>630</sub> was measured at the beginning and after 20 or 90 min at 25 °C. Absorbance after 20 or 90 min was plotted against the protein concentration. Matlab (Mathworks, USA) was used to fit a logistic function to the data. The midpoint value of the function was used as EC<sub>50</sub>.

### 2.4. Lipid vesicle preparation

All lipids were purchased from Avanti Polar Lipids, USA, and used without further purification. Lipids were dissolved and mixed in chloroform at indicated molar ratios. The thin lipid film was produced using a rotavapor (Büchi, Switzerland) and subsequently subjected to a high vacuum for a minimum duration of 2 h.

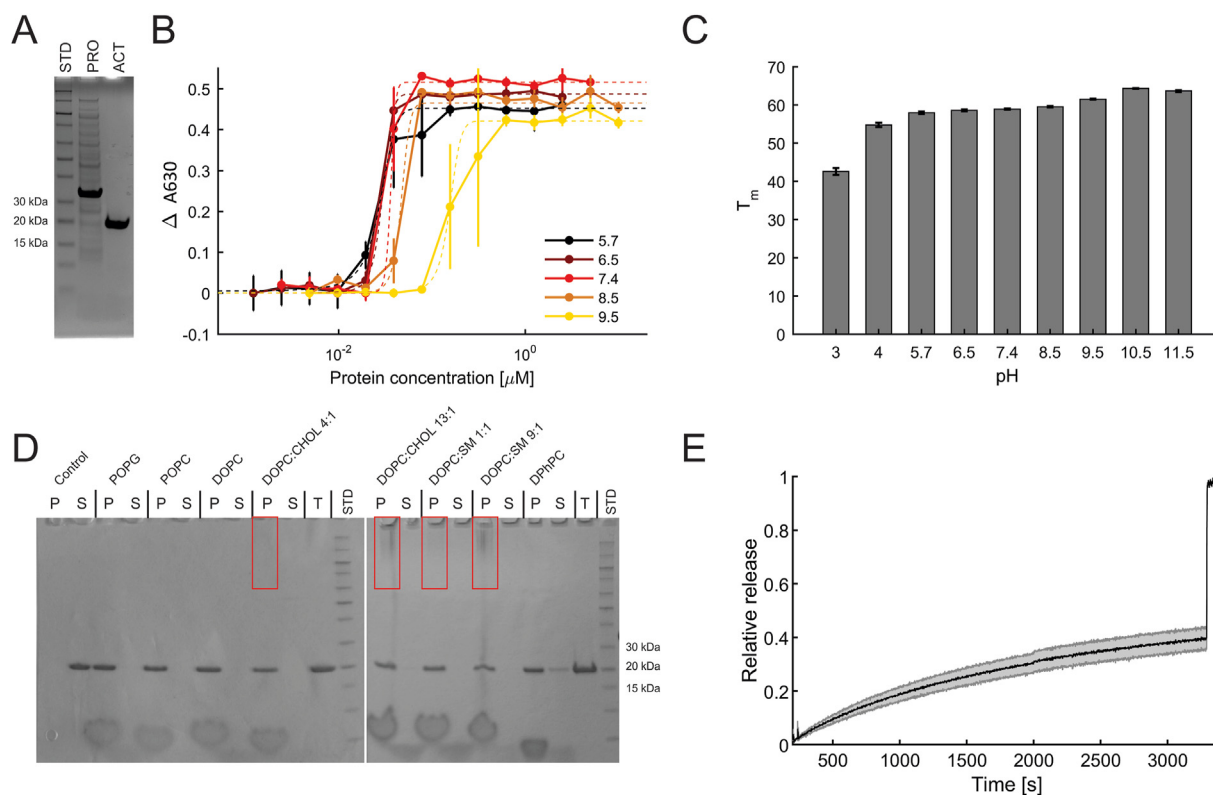


**Fig. 1.** Interaction of Cyt2Aa with model lipid membranes. (A) SDS-PAGE of recombinant Cyt2Aa in protoxin (PRO) and activated (ACT) form. STD: molecular weight standard. (B) Hemolytic activity of Cyt2Aa at different pH values. Each measurement was repeated three times. Points represent mean value  $\pm$  SD; Dashed lines are sigmoidal functions fitted to the data used in  $EC_{50}$  estimation. (C) The thermal stability of Cyt2Aa measured by differential scanning fluorimetry at indicated pH values. Each  $T_m$  value shown is the mean value  $\pm$  SD of three independent experiments. (D) SDS-PAGE analysis of Cyt2Aa binding to MLVs as determined by lipid sedimentation assay. All lipid compositions are in molar ratios. Control is the same experiment performed in the absence of MLVs. P, pellet; S, supernatant; T, total protein; STD, molecular weight standard. Red rectangles highlight high molecular weight protein species. (E) Kinetics of calcein release from 20  $\mu$ M DOPC LUVs induced by 2.5  $\mu$ M Cyt2Aa. The bold central line is an average of three measurements, the shaded area shows SD.

Multilamellar vesicles (MLVs) were prepared by hydrating the lipid film in PBS or MilliQ water at 22–24 °C and vigorous vortexing together with 0.5 mm glass beads to re-suspend the lipids, followed by three cycles of freezing and thawing in liquid nitrogen. Large unilamellar vesicles (LUVs) were prepared from the MLVs by extrusion using LiposoFast lipid extruder (Avestin, Canada) through polycarbonate membranes with 100 nm pores.

### 2.5. Calcein release assay

Calcein release assay was performed as described before [46] with minor modifications. Permeabilization of 20  $\mu$ M calcein-loaded LUVs by Cyt2Aa was measured with QuantaMaster 400 (Photon Technology International, USA) at 485 nm and 520 nm excitation and emission wavelengths, respectively. 200 s after the beginning of the measurement 2.5  $\mu$ M Cyt2Aa was added to 20  $\mu$ M LUVs. The release of calcein was followed for 3600 s, at which point, mM Triton X-100 was added to achieve 100% calcein release.

### 2.6. Lipid sedimentation assay

4  $\mu$ M of Cyt2Aa were mixed with MLVs (5 mM) in PBS and incubated for 30 min at room temperature. The negative control experiment was performed using PBS instead of MLVs. The mixture was centrifuged for 30 min at 16100 $\times$ g. After this, the supernatant was removed and stored for later analysis with SDS-PAGE. The pellet was washed twice by resuspension with PBS and subsequent centrifugation for an additional 20 min at 16100 $\times$ g. Supernatant in

wash steps was discarded. The final pellet and supernatant were subjected to SDS-PAGE, followed by SimplyBlue SafeStain (Thermo Fisher Scientific, USA) staining.

### 2.7. Oligomerization assays and oligomer visualization with Native-PAGE

5.6  $\mu$ M of activated Cyt2Aa was incubated with 5 or 10 mM 1,2-dioleoyl-*sn*-glycero-3-phosphocholine (DOPC) :cholesterol (CHOL) (13:1) MLVs. After incubation vesicles were solubilized with 2% Triton X-100. Additionally, the same amount of protein was incubated with detergents (0.25 mM Brij 35-, 5-, 10-, and 20 mM Triton X-100, 10- and 20 mM Fos-choline-12, 10- and 20 mM Fos-choline-16, and 10 and 20 mM n-dodecyl  $\beta$ -D-maltoside). Samples were subjected to Native-PAGE analysis.

### 2.8. Cryo-electron microscopy (cryo-EM) sample preparation and data collection

MLVs were prepared in PBS, as described above. The activated form of Cyt2Aa was added to MLVs, at the final concentration of 500 nM and 10 mM, respectively, and the mixture was incubated for 30 min at room temperature. In one experiment the vesicles exposed to Cyt2Aa were solubilized with 2% Triton X-100. In the third case the sample was prepared by incubation of 2  $\mu$ M Cyt2Aa with 0.25 mM solution of Brij 35 in PBS. In all three cases 3  $\mu$ l of suspension was applied to Quantifoil R1.2/1.3300-mesh copper holey carbon grid (Quantifoil, Germany) that were glow-discharged

using (GloQube® Plus, Quorum, UK). The grids were blotted under 100% humidity at 4 °C for 6–7 s and plunged into liquid ethane using a Mark IV Vitrobot (Thermo Fisher Scientific, USA). Micrographs were recorded with a cryo-transmission electron microscope operating at 200 kV (Glacios, Thermo Fisher Scientific, USA) with a Falcon 3 EC direct electron detector (Thermo Fisher Scientific, USA) using the EPU software (Thermo Fisher Scientific, USA). Images were recorded in counting mode with the pixel size of 0.98 and 0.47 Å. Micrographs were dose-fractionated into 38 frames with total dose of 30 e<sup>-</sup>/Å.

### 2.9. Cryo-EM image processing

All steps of data processing were performed in cryoSPARC 2.4 with built-in algorithms [47]. Cryo-EM data analysis followed the typical steps of a single-particle analysis protocol, stopping at Ab-initio reconstruction. Movies were aligned and contrast transfer function estimation was performed. Particles were initially picked by hand and 2D classified to create 2D class averages used in template picking. Particles picked in this way underwent several rounds of 2D classification to produce final 2D classes. 3D volume was generated with an Abinitio reconstruction.

### 2.10. Circular dichroism spectroscopy

Circular dichroism (CD) spectra were collected on Chirascan CD Spectrometer (Applied Photophysics, UK). Proteins were 20 times diluted in the respective buffers to a final concentration of 0.2 mg/ml. Dilution buffers were MilliQ water, solution of 0.25 mM Brij 35 and, suspension of 5 mM DOPC:CH 13:1 LUVs. These buffers were also used as controls and their spectra was subtracted from the spectra of the corresponding protein samples. Protein spectra were measured at 25 °C, over the wavelength range 250–195 nm, using an interval of 1 nm and a dwell time of 1 s, with ten repeat scans of each sample.

## 3. Results

### 3.1. Recombinant Cyt2Aa permeabilizes model lipid membranes of various compositions

The recombinant pro-toxin form of Cyt2Aa was produced in *E. coli*. The inactive pro-form of Cyt2Aa was treated with 1% (w/w) proteinase K to obtain an active toxin (Fig. 1A), which was further purified using size exclusion chromatography. After activation additional step of size-exclusion chromatography was performed to separate the active form of Cyt2Aa from proteinase K and other impurities. The cytolytic activity of Cyt2Aa was assessed by a hemolysis assay using bovine red blood cells (RBCs) at different pH values. At all pH values tested, the hemolytic activity of Cyt2Aa showed a sigmoidal dependence on protein concentration (Fig. 1B). The hemolytic activity was highest at neutral and acidic conditions and decrease significantly at pH values above 8.5 with estimated EC<sub>50</sub>s of 0.027 ± 0.005 μM, 0.030 ± 0.002 μM, 0.037 ± 0.003 μM, 0.043 ± 0.006 μM, and 0.157 ± 0.088 μM for pH values of 5.7, 6.5, 7.4, 8.5 and 9.5, respectively. This was rather unexpected as the physiologically relevant pH of the midgut of insects is 10.5 [48]. On the other hand, the thermal stability test showed that the stability of Cyt2Aa increased with pH, as expected (Fig. 1C).

Cyt proteins generally bind to most lipid membranes and require unsaturated fatty acids for binding [9]. We tested the binding of Cyt2Aa to multi lamellar vesicles (MLVs) composed of several common lipids (Fig. 1D). We also used DOPC - cholesterol vesicles with the molar ratio DOPC: CHOL 13:1, as such lipid bilayers have been used in previous studies of Cyt2Aa [49]. As

expected, Cyt2Aa bound to all types of MLVs to a comparable extent (Fig. 1D). In MLVs where DOPC was supplemented with sphingomyelin (SM) or CHOL, we also observed smears on SDS-PAGE gels corresponding to larger Cyt2Aa complexes. Interestingly, we also observed binding to 1,2-diphytanoyl-*sn*-glycero-3-phosphocholine (DPhPC) with diphytanoyl fatty acid chains (Fig. 1D).

To validate the membrane disrupting activity of Cyt2Aa on a simple one component membrane system, we performed a calcein release experiment on large unilamellar vesicles (LUVs) of DOPC (Fig. 1D). After the addition of 2.5 μM Cyt2Aa, the release of calcein from the vesicles was slow and did not reach a plateau after 1 h.

### 3.2. Cyt2Aa forms oligomers in the presence of lipid membranes or detergents

Cyt2Aa forms detergent-resistant oligomers upon exposure to lipid membranes [35]. Structural characterization of the oligomers is a crucial step towards understanding the membrane-disrupting mechanism. To prepare Cyt2Aa in oligomeric form for further structural and functional analysis, we incubated Cyt2Aa with DOPC:CHOL (13:1) MLVs at 22 °C and solubilized the vesicles with Triton X-100 after different incubation times. We also incubated Cyt2Aa with detergents Triton X-100 or Brij 35 and observed the formation of oligomers on Native-PAGE (Fig. 2A). When Cyt2Aa was incubated with MLVs, the band corresponding to the monomer disappeared and multiple bands of higher oligomers appeared. Bands corresponding to larger oligomers were also found when Cyt2Aa was incubated with Triton X-100 or Brij 35, but in this case, the band corresponding to a monomer was much more pronounced (Fig. 2A). To test how incubation time affects oligomer size, we incubated Cyt2Aa with DOPC:CHOL (13:1) MLVs for 5, 15, 30 and 45 min. After incubation, the vesicles were solubilized as described above and analyzed by native-PAGE, which showed that the size of the oligomers increased with time (Fig. 2B).

### 3.3. Cyt2Aa forms filamentous oligomers on the lipid membrane surface

Two types of samples were first visualized using Cryo-EM. A Cyt2Aa sample incubated with DOPC:CHOL (13:1) MLVs and a sample where the MLVs were solubilized with a detergent after incubation with Cyt2Aa. The membranes of MLVs that were not treated Cyt2Aa (control) were smooth and undamaged (Fig. 2C). After incubation of the MLVs with Cyt2Aa, we found the protein bound to the outer surface of all observed lipid vesicles (Fig. 2D). In addition to the protein bound to the membranes, a large number of linear protein filaments, heterogeneous in length, in line with Fig. 2A and B were present in the vicinity of the vesicles. These filaments were picked to create 2D class averages (Fig. 2D, bottom), showing that the filaments were composed of a single row of proteins. As expected, similar filaments were also present in the second sample in which the Cyt2Aa-bound vesicles were solubilized with detergent (Fig. 2E). The 2D class averages of the filaments are also comparable in size and shape between the two samples (Fig. 2D and E, bottom).

We also noted another type of oligomers that was clearly visible near or on the membranes of the lipid vesicles (Fig. 3A). Compared to the linear filamentous oligomers described above, these were shorter and had more curvature. Whereas linear filamentous oligomers (white arrows) were mainly found in solution and partly on membranes, the shorter curved oligomers (black arrows) were mostly found on or in close proximity to membranes (Figs. 2D and 3A and B). *Ab initio* 3D-reconstruction of the linear filamentous oligomers also suggests that Cyt2Aa oligomerization involves the formation of single-row filaments composed of Cyt2Aa subunits

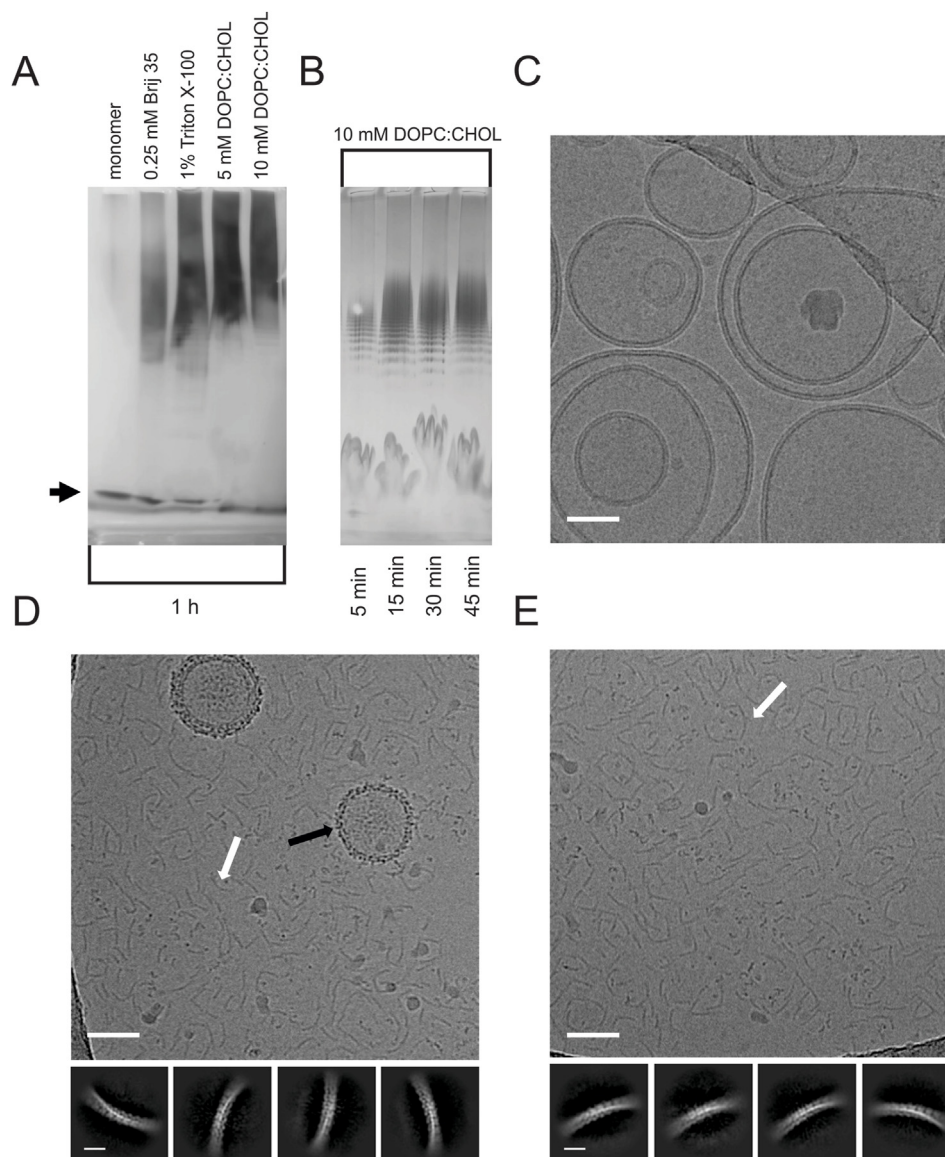


**Fig. 2.** Visualization of Cyt2Aa oligomers. (A,B) Silver-stained Native-PAGE gel of Cyt2Aa. (A) 5.6  $\mu\text{M}$  of monomeric Cyt2Aa was subjected to different treatments: Untreated monomer, Cyt2Aa incubated for 1 h with 0.25 mM Brij 35 or with 1% Triton X-100, and incubated for 1 h with 5 and 10 mM DOPC:CHOL (13:1) MLVs (respectively). A black arrow marks the band corresponding to monomeric Cyt2Aa. (B) Cyt2Aa incubated for indicated times with 10 mM DOPC:CHOL (13:1) MLVs. Samples were solubilized with 1% Triton X-100 and incubated at 22  $^{\circ}\text{C}$ . (C) Control: cryo-EM micrograph of DOPC:CHOL (13:1) MLVs in the absence of Cyt2Aa (D) Top: representative micrograph of Cyt2Aa incubated with DOPC:CHOL (13:1) MLVs recorded with cryo-EM. White arrows points at the filamentous oligomer; the black arrow points at an MLV with protein bound to the membrane. Below: 2D classes of Cyt2Aa oligomers. (E) Top: representative micrograph of Cyt2Aa incubated with DOPC:CHOL (13:1) MLVs followed by solubilization with 1% DDM. White arrow points to an example of a filamentous oligomer. Below: 2D classes of Cyt2Aa oligomers. The scale bar on micrographs (C–E) is 50 nm and 6 nm on 2D classes (D, E).

(Fig. 3C). In addition, we captured several vesicles at the moment of rupture (Fig. 3B, red arrows indicate ruptured membranes), with filamentous oligomers (Fig. 3B, white arrows) distributed between the ends of ruptured membranes (Fig. 3B, white lines indicating the distribution of the filaments).

#### 3.4. Structurally similar oligomeric Cyt2Aa filaments are formed when the protein is exposed to lipids or detergents

As shown in Fig. 2A, Cyt2Aa forms oligomers in the presence of detergents in absence of lipid vesicles. To investigate this further, we examined how different detergents affect oligomerization. We incubated Cyt2Aa with Brij 35, Triton X-100, Fos-Choline-12, Fos-Choline-16, and n-dodecyl  $\beta$ -D-maltoside (DDM) all of which induced oligomerization, albeit to varying degrees as analyzed by

Native-PAGE (Fig. 4A). We then imaged Cyt2Aa incubated with Brij 35 using cryo-EM. The oligomers formed by Cyt2Aa (Fig. 4B) looked similar to the linear filamentous oligomers observed when MLVs were incubated with Cyt2Aa before and after solubilization with detergent (Fig. 2D and E).

To test whether the conformation changes during oligomerization, we recorded CD spectra of Cyt2Aa under different conditions. When comparing the spectrum of monomeric Cyt2Aa in water with that of Cyt2Aa incubated with Brij 35, the two differ significantly with the latter indicating a higher proportion of  $\alpha$ -helices. The CD spectrum of the sample with MLVs differs from both with a higher signal in the  $\alpha$ -helical region of the spectrum than for monomeric Cyt2Aa, but not as strong as that of Cyt2Aa incubated with Brij 35. This could be due to the presence of the conformational intermediates present on the membrane surface or a mixture of

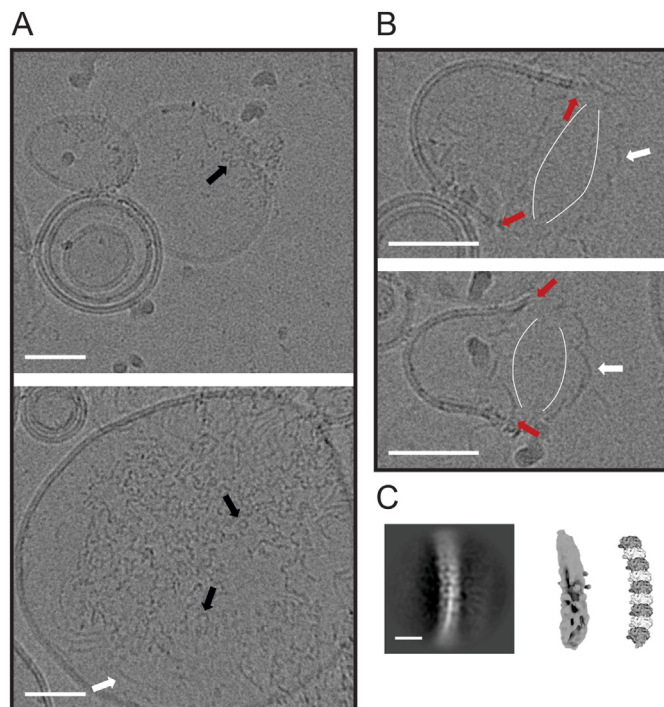


**Fig. 3.** Two types of oligomers are present on and around the vesicles. (A) Two representative micrographs of vesicles with Cyt2Aa bound to the membrane. Scale bar is 50 nm; (B) Two representative micrographs of ruptured vesicles with two rows of filamentous Cyt2Aa oligomers in the vicinity of the rupture. Scale bar is 50 nm. Black arrows point at shorter oligomers with higher curvature, white arrow points at more linear oligomers, and red arrows point at the ends of disrupted membranes. The white lines indicate the two rows of filamentous oligomers connecting the ends of the ruptured vesicle; (C) Close-up of a 2D class average of the filamentous oligomer with clear segmentation (left; scale bar is 6 nm). 3D volume of the filament obtained after Ab-initio reconstruction (middle), and a suggested model of the oligomer based on the 2D class (C) and crystal structure of the Cyt2Aa monomer (PDB id: 1CBY). Alternating Cyt2Aa subunits shown as molecular surfaces are colored differently (light or dark grey) to better demonstrate the oligomeric structure.

conformational states.

We then tested the hemolytic activity of the filamentous oligomers formed by Cyt2Aa after inducing the oligomerization by pre-incubating Cyt2Aa with 0.25 mM Brij 35 or 0.15 mM DDM. To maintain the oligomeric state of Cyt2Aa during the subsequent hemolysis assay, the PBS buffer had to contain equal amounts of detergent, i.e. 0.25 mM Brij 35 or 0.15 mM DDM. This was problematic as both detergents showed some degree of hemolytic activity in the control experiment without Cyt2Aa. In the case where Cyt2Aa was pre-incubated in Brij 35 and the activity of the control was subtracted, we did not detect any hemolytic effect of the protein (Fig. 4E grey line). The control buffer with DDM caused complete hemolysis, so a similar approach was not possible. To solve this problem, we performed a second set of experiments in which we pre-incubated a high concentration of Cyt2Aa with Brij 35 or DDM and then diluted the sample 16 times with a detergent-free buffer. Subsequently, we performed further serial dilutions of Cyt2Aa to the final concentrations indicated in Fig. 4D and measured hemolytic activity. In this case, we observed no hemolytic activity in the control measurements in the absence of Cyt2Aa. We observed lower hemolytic activity of detergent pre-treated Cyt2Aa compared to the case where Cyt2Aa was not treated with detergents (Fig. 4E) with estimated  $EC_{50}$ s of  $0.032 \pm 0.003 \mu\text{M}$ ,  $0.066 \pm 0.005 \mu\text{M}$ , and  $0.103 \pm 0.006 \mu\text{M}$  for untreated Cyt2Aa, Brij 35-treated Cyt2Aa and DDM-treated Cyt2Aa, respectively. This suggests Cyt2Aa oligomers have very low or even no hemolytic

activity and that the observed activity of Cyt2Aa pre-treated with detergents and subsequently diluted in buffer without detergents is due to the dissociation of oligomers caused by the low detergent concentration.

#### 4. Discussion

*Bt* is a commonly used bioinsecticide. The toxic agents of its insecticidal activity are the parasporal proteins [3–5]. To better understand the molecular mechanism behind the biological activity of the toxin Cyt2Aa, we have investigated the activity of Cyt2Aa towards different model membrane systems, focusing on the visualization and structural reconstruction of Cyt2Aa oligomers.

We have found that the hemolytic activity of Cyt2Aa is best at neutral and acidic pH. While this may be counterintuitive, as the high pH of 10.5 [48] of the insect midgut is required for solubilization of Cyt toxins, the activity is not necessarily linked to the midgut and could also play a role in the hindgut. Moreover, the concentration of Cyt2Aa required to induce hemolysis was high, especially when compared to potent pore-forming proteins such as cnidarian actinoporin FraC, where successful hemolysis is achieved at concentrations 100-fold lower than those of Cyt2Aa under the same conditions [46]. To complement the hemolysis assay, we performed a calcein release assay, which in agreement with hemolysis, showed that membrane disruption by Cyt2Aa is slow and requires high concentrations of the protein.

Using cryo-EM we analyzed oligomer formation by Cyt2Aa under three different conditions, (i) Cyt2Aa incubated with DOPC:CHOL (13:1) MLVs, (ii) Cyt2Aa incubated with DOPC:CHOL (13:1) MLVs followed by vesicle solubilization with detergents, and (iii) Cyt2Aa incubated with a detergent Brij 35. In all three cases, we observed filamentous oligomers in solution. The 2D class averages of filamentous oligomers between the three samples were comparable in size and shape. From the 2D averages, we can clearly see the segmentation and that the oligomer consists of a single row of Cyt2Aa protomers (Fig. 3C). At a level of micrographs, Cyt2Aa oligomers are morphologically similar to oligomers observed previously for Cyt1Aa [23] and for the fungal volvatoxin A2, which is structurally related to Cyt2Aa [50], with cryo-EM and negative stain TEM respectively. In contrast to the filamentous oligomers primarily found in solution, we observed other, shorter, oligomers with higher curvature on the MLVs, located almost exclusively on the lipid membranes (Figs. 2D and 3A). In addition, we observed several cases where two lines of filamentous oligomers connected a ruptured vesicle lipid membrane (Fig. 3B), suggesting that the oligomers transform into more linear filaments after dissociation from the membrane.

Interestingly, incubation of Cyt2Aa with detergents in the absence of membranes leads to the formation of similar linear filamentous oligomers. Combined with results of CD spectroscopy, this suggests that Cyt2Aa may have different conformations in its soluble monomeric form compared to the oligomeric membrane-bound form or solubilized filamentous oligomer. When we tested the hemolytic activity of Cyt2Aa pre-incubated with detergents its activity was reduced, which, in combination with our cryo-EM results, suggesting that these cytolytically inactive filamentous oligomers may represent the final step in the membrane-disrupting process.

Based on our results, we propose the following model of action (Fig. 5): The monomeric form of activated Cyt2Aa binds to the membrane. There it oligomerizes and forms curved complexes on the lipid membrane surface. According to previously published data [9,44,51,52], these complexes are partially inserted into the membrane. After reaching a critical local concentration, the membrane bursts and the oligomers are released from the membrane.

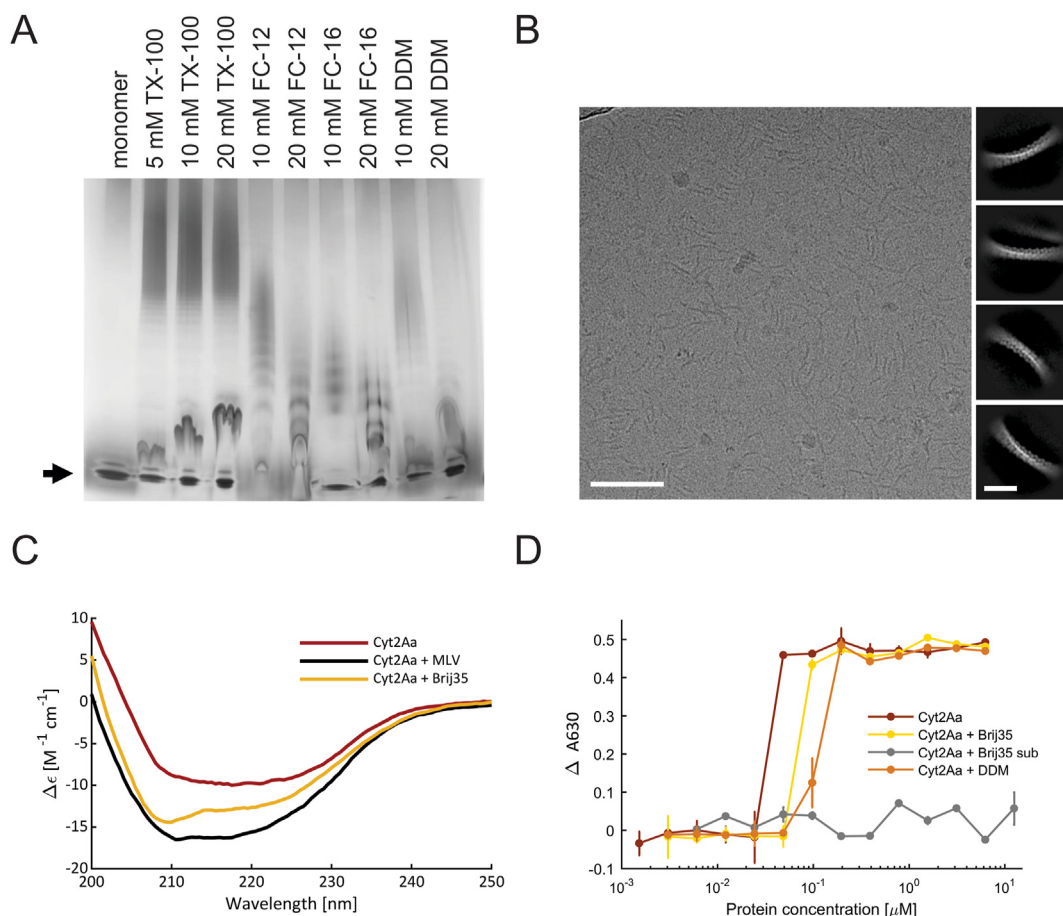


**Fig. 4.** Detergents trigger Cyt2Aa oligomerization. (A) Silver-stained Native-PAGE gel of Cyt2Aa oligomers induced by detergents Triton X-100 (TX-100), Fos-Choline-12 (FC-12), Fos-Choline-16 (FC-16), and dodecylmaltoside (DDM). 5.6  $\mu M$  of monomeric Cyt2Aa was incubated with indicated detergents for 30 min at room temperature. A black arrow marks the band corresponding to monomeric Cyt2Aa. (B) Left: Representative cryo-EM micrograph of Cyt2Aa incubated with Brij 35. The scale bar is 50 nm. Right: 2D classes of Cyt2Aa oligomers, the scale bar is 8 nm; (D) CD spectra of monomeric Cyt2Aa, Cyt2Aa incubated with DOPC:CHOL (13:1) MLVs and Cyt2Aa incubated with Brij 35; (E) Hemolytic activity of Cyt2Aa after incubation with Brij 35 and DDM. Preincubated proteins were at least 16 x times diluted in PBS. The grey line shows the change in absorbance at 630 nm ( $A_{630}$ ) of Cyt2Aa incubated in Brij 35 and then serially diluted (1:1) in PBS buffer with 0.25 mM Brij 35. The effect of PBS buffer containing an equal concentration of Brij 35 was subtracted from the observed change in  $A_{630}$  after 90 min. Points represent mean value  $\pm$  SD of 3 or 4 experiments.

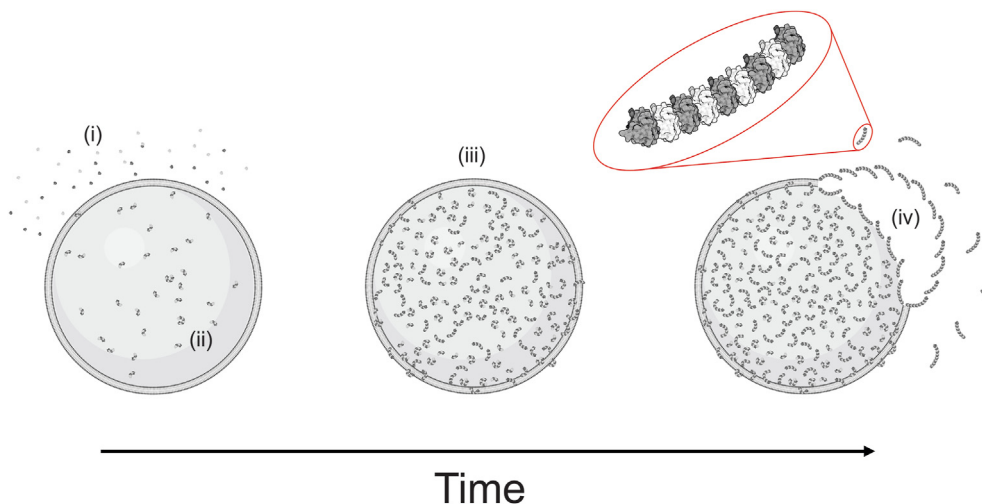


**Fig. 5.** Schematic representation of the suggested model of Cyt2Aa membrane disruption. We propose a four-step membrane-disruption process: (i) Monomeric Cyt2Aa binds the lipid bilayer. (ii) Upon exposure to a hydrophobic environment, it undergoes a conformational change and oligomerizes. Initial oligomers are short and curved. (iii) With time or upon reaching a critical concentration, the oligomers become longer and more linear and (iv) solubilize the membrane and get released into the solution.

When they are no longer immersed in the hydrophobic environment of the membrane, they may undergo a conformational change and form filamentous oligomers that are no longer cytolytically active (Fig. 4 D). Our results do not support the typical model of transmembrane pore formation mechanism [39], as we do not see any evidence of a formation of ring or arc-shaped functional transmembrane pores by Cyt2Aa. Instead, we suggest that Cyt2Aa ruptures membranes through a rather complex mode of action that is consistent with a detergent-like mechanism of action [45].

Alternatively, the poor ability to disrupt membranes, combined with the broad membrane binding specificity makes Cyt2Aa the perfect cofactor for other cytolytic proteins in the broad arsenal of *Bt*. Synergistic interactions between Cyt and Cry toxins have been previously described for Cyt1Aa [14,15], Cyt2Aa [13] and Cyt2Ba [12]. The cytolytic activity of Cyt toxins could be a secondary effect, and their primary function that of a membrane-binding partner in a two- or multicomponent protein complex, as previously suggested [23]. This, together with the fact that Cyt toxins do not require a protein receptor [29], makes them a great option for circumventing evolving insect resistance [6,53], where mutations at protein receptors would render Cry proteins useless on their own.

### Author contributions

GŠ., GA., and MP. designed the experiments. GŠ performed all the experiments. GŠ., GA. and MP all wrote and revised the manuscript.

### Funding

This work was supported by the Slovenian Research Agency (Program grant Molecular Interactions P1-0391 and Infrastructure Program IO-0003) and Oxford Nanopore Technologies Limited.

### Declaration of competing interest

The authors declare that they have no known competing financial interests or personal relationships that could have appeared to influence the work reported in this paper.

### Acknowledgements

The authors would like to thank Tomaž Švigelj for technical assistance.

### References

- [1] A. Bravo, S. Likitvivanavong, S.S. Gill, M. Soberón, *Bacillus thuringiensis*: a story of a successful bioinsecticide, *Insect Biochem. Mol. Biol.* 41 (2011) 423–431, <https://doi.org/10.1016/j.ibmb.2011.02.006>.
- [2] E.N. Santos, L.P. Menezes, S.S. Dolabella, A. Santini, P. Severino, R. Capasso, A. Zielinska, E.B. Souto, S. Jain, *Bacillus thuringiensis*: from biopesticides to anticancer agents, *Biochimie* 192 (2022) 83–90, <https://doi.org/10.1016/j.biochi.2021.10.003>.
- [3] E. Schnepf, N. Crickmore, J. Van Rie, D. Lereclus, J. Baum, J. Feitelson, D.R. Zeigler, D.H. Dean, *Bacillus thuringiensis* and its pesticidal crystal proteins, *Microbiol. Mol. Biol. Rev.* 62 (1998) 775–806, <https://doi.org/10.1128/mmr.62.3.775-806.1998>.
- [4] H. Hofte, H.R. Whiteley, Insecticidal crystal proteins of *Bacillus thuringiensis*, *Microbiol. Rev.* 53 (1989) 242–255, <https://doi.org/10.1128/mmr.53.2.242-255.1989>.
- [5] N. Crickmore, D.R. Zeigler, J. Feitelson, E. Schnepf, J. Van Rie, D. Lereclus, J. Baum, D.H. Dean, Revision of the nomenclature for the *Bacillus thuringiensis* pesticidal crystal proteins, *Microbiol. Mol. Biol. Rev.* 62 (1998) 807–813, <https://doi.org/10.1128/mmr.62.3.807-813.1998>.
- [6] L. Pardo-López, M. Soberón, A. Bravo, *Bacillus thuringiensis* insecticidal three-domain Cry toxins: mode of action, insect resistance and consequences for crop protection, *FEMS Microbiol. Rev.* 37 (2013) 3–22, <https://doi.org/10.1111/j.1574-6976.2012.00341.x>.
- [7] Crickmore, N., Berry, C., Panneerselvam, S., Mishra, R., T.R. Connor, B.C. Bonning, Bacterial Pesticidal Protein Resource Center, (n.d.). <https://www.bpprc.org>.
- [8] N. Crickmore, C. Berry, S. Panneerselvam, R. Mishra, T.R. Connor, B.C. Bonning, A structure-based nomenclature for *Bacillus thuringiensis* and other bacteria-derived pesticidal proteins, *J. Invertebr. Pathol.* 186 (2021), 107438, <https://doi.org/10.1016/j.jip.2020.107438>.
- [9] P. Butko, Cytolytic toxin Cyt1A and its mechanism of membrane damage: data and hypotheses, *Appl. Environ. Microbiol.* 69 (2003) 2415–2422, <https://doi.org/10.1128/AEM.69.5.2415-2422.2003>.
- [10] J. Li, P. a Koni, D.J. Ellar, Structure of the mosquitoicidal delta-endotoxin CytB from *Bacillus thuringiensis* sp. *kyushuensis* and implications for membrane pore formation, *J. Mol. Biol.* 257 (1996) 129–152, <https://doi.org/10.1006/jmbi.1996.0152>.
- [11] J. Li, J. Carroll, D.J. Ellar, Crystal structure of insecticidal  $\delta$ -endotoxin from *Bacillus thuringiensis* at 2.5 Å resolution, *Nature* 353 (1991) 815–821, <https://doi.org/10.1038/353815a0>.
- [12] D. Valtierra-De-Luis, M. Villanueva, L. Lai, T. Williams, P. Caballero, Potential of Cry10Aa and Cyt2Ba, two minority  $\delta$ -endotoxins produced by *Bacillus thuringiensis* ser. israelensis, for the control of *Aedes aegypti* larvae, *Toxins* 12 (2020) 1–14, <https://doi.org/10.3390/toxins12060355>.
- [13] B. Promdonkoy, P. Promdonkoy, S. Panyim, Co-expression of *Bacillus thuringiensis* Cry4Ba and Cyt2Aa2 in *Escherichia coli* revealed high synergism against *Aedes aegypti* and *Culex quinquefasciatus* larvae, *FEMS Microbiol. Lett.* 252 (2005) 121–126, <https://doi.org/10.1016/j.femsle.2005.08.038>.
- [14] A. Hernández-Soto, M.C. Del Rincón-Castro, A.M. Espinoza, J.E. Ibarra, Parasporal body formation via overexpression of the Cry10Aa toxin of *Bacillus thuringiensis* subsp. israelensis, and Cry10Aa-Cyt1Aa synergism, *Appl. Environ. Microbiol.* 75 (2009) 4661–4667, <https://doi.org/10.1128/AEM.00409-09>.
- [15] C. Pérez, C. Muñoz-Garay, L.C. Portugal, J. Sánchez, S.S. Gill, M. Soberón, A. Bravo, *Bacillus thuringiensis* ssp. israelensis Cyt1Aa enhances activity of Cry11Aa toxin by facilitating the formation of a pre-pore oligomeric structure, *Cell. Microbiol.* 9 (2007) 2931–2937, <https://doi.org/10.1111/j.1462-5822.2007.01007.x>.
- [16] B.A. Federici, L.S. Bauer, Cyt1Aa protein of *Bacillus thuringiensis* is toxic to the cottonwood leaf beetle, *Chrysomela scripta*, and Suppresses High Levels of Resistance to Cry3Aa 64 (1998) 4368–4371.
- [17] M. Helena, N. Lobo, T. Patricia, T. Maria, T. Rezende, S. Carvalho, H. Suzany, G. De Menezes, N. Alexandre, M. Sober, A. Bravo, Bacterial toxins active against mosquitoes: mode of action and resistance, *Toxins* 13 (2021) 523, <https://doi.org/10.3390/toxins13080523>.
- [18] M. Soberón, J.A. López-Díaz, A. Bravo, Cyt toxins produced by *Bacillus thuringiensis*: a protein fold conserved in several pathogenic microorganisms, *Peptides* 41 (2013) 87–93, <https://doi.org/10.1016/j.peptides.2012.05.023>.
- [19] C. Pérez, L.E. Fernandez, J. Sun, J.L. Folch, S.S. Gill, M. Soberón, A. Bravo, *Bacillus thuringiensis* subsp. israelensis Cyt1Aa synergizes Cry11Aa toxin by functioning as a membrane-bound receptor, *Proc. Natl. Acad. Sci. U.S.A.* 102 (2005), 18303, <https://doi.org/10.1073/PNAS.0505494102>.
- [20] L. Palma, D. Muñoz, C. Berry, J. Murillo, P. Caballero, P. Caballero, *Bacillus thuringiensis* toxins: an overview of their biocidal activity, *Toxins* 6 (2014) 3296–3325, <https://doi.org/10.3390/toxins6123296>.
- [21] B.H. Knowles, P.J. White, C.N. Nicholls, D.J. Ellar, A broad-spectrum cytolytic toxin from *Bacillus thuringiensis* var. *kyushuensis*, *Proc. Biol. Sci.* 248 (1992) 1–7, <https://doi.org/10.1098/rspb.1992.0035>.
- [22] P.A. Koni, D.J. Ellar, Cloning and characterization of a novel *Bacillus thuringiensis* cytolytic delta-endotoxin, *J. Mol. Biol.* (1993) 319–327.
- [23] G. Tetreau, A.S. Banneville, E.A. Andreeva, A.S. Brewster, M.S. Hunter, R.G. Sierra, J.M. Teulon, I.D. Young, N. Burke, T.A. Grünwald, J. Beaudouin, I. Snigireva, M.T. Fernandez-Luna, A. Burt, H.W. Park, L. Signor, J.A. Bafna, R. Sadrir, D. Fenel, E. Boeri-Erba, M. Bacia, N. Zala, F. Laporte, L. Després, M. Weik, S. Boutet, M. Rosenthal, N. Coquelle, M. Burghammer, D. Cascio, M.R. Sawaya, M. Winterhalter, E. Gratton, I. Gutsche, B. Federici, J.L. Pellequer, N.K. Sauter, J.P. Colletier, Serial femtosecond crystallography on in vivo-grown crystals drives elucidation of mosquitoicidal Cyt1Aa bioactivation cascade, *Nat. Commun.* 11 (2020), <https://doi.org/10.1038/s41467-020-14894-w>.
- [24] S. Cohen, O. Dym, S. Albeck, E. Ben-Dov, R. Cahan, M. Firer, A. Zaritsky, High-Resolution crystal structure of activated Cyt2Ba monomer from *Bacillus thuringiensis* subsp. israelensis, *J. Mol. Biol.* 380 (2008) 820–827, <https://doi.org/10.1016/j.jmb.2008.05.010>.
- [25] S. Cohen, S. Albeck, E. Ben-Dov, R. Cahan, M. Firer, A. Zaritsky, O. Dym, Cyt1Aa toxin: crystal structure reveals implications for its membrane-perforating function, *J. Mol. Biol.* 413 (2011) 804–814, <https://doi.org/10.1016/j.jmb.2011.09.021>.
- [26] S.A.S. Al-yahyaee, D.J. Ellar, Maximal toxicity of cloned CytA  $\delta$ -endotoxin from *Bacillus thuringiensis* subsp. israelensis requires proteolytic processing from both the N- and C-termini, *Microbiology* 141 (1995) 3141–3148, <https://doi.org/10.1099/13500872-141-12-3141>.
- [27] P.A. Koni, D.J. Ellar, Biochemical characterization of *Bacillus thuringiensis* cytolytic  $\delta$ -endotoxins, *Microbiology* 140 (1994) 1869–1880, <https://doi.org/10.1099/13500872-140-8-1869>.
- [28] R. Cahan, H. Friman, Y. Nitzan, Antibacterial activity of Cyt1 Aa from *Bacillus thuringiensis* subsp. israelensis, *Microbiology* 154 (2008) 3529–3536, <https://doi.org/10.1099/mic.0.2008/020784-0>.
- [29] W.E. Thomas, D.J. Ellar, Mechanism of action of *Bacillus thuringiensis* var. israelensis insecticidal delta-endotoxin, *FEBS Lett.* 154 (1983) 362–368.
- [30] A. Moreno-Cencerrado, S. Tharad, J. Iturri, B. Promdonkoy, C. Krittanai,

- J.L. Toca-Herrera, Time influence on the interaction between Cyt2Aa2 and lipid/cholesterol bilayers, *Microsc. Res. Tech.* 79 (2016) 1017–1023, <https://doi.org/10.1002/jemt.22736>.
- [31] S.H. Maddrell, N.J. Lane, J.B. Harrison, J.A. Overton, R.B. Moreton, The initial stages in the action of an insecticidal delta-endotoxin of *Bacillus thuringiensis* var. *israelensis* on the epithelial cells of the malpighian tubules of the insect, *Rhodnius prolixus*, *J. Cell Sci.* 90 (Pt 1) (1988) 131–144.
- [32] S.H. Maddrell, J.A. Overton, D.J. Ellar, B.H. Knowles, Action of activated 27,000 Mr toxin from *Bacillus thuringiensis* var. *israelensis* on Malpighian tubules of the insect, *Rhodnius prolixus*, *J. Cell Sci.* 94 (Pt 3) (1989) 601–608. [http://www.ncbi.nlm.nih.gov/entrez/query.fcgi?cmd=Retrieve&db=PubMed&dopt=Citation&list\\_uids=2632587](http://www.ncbi.nlm.nih.gov/entrez/query.fcgi?cmd=Retrieve&db=PubMed&dopt=Citation&list_uids=2632587).
- [33] A. Bravo, S.S. Gill, M. Soberón, Mode of action of *Bacillus thuringiensis* Cry and Cyt toxins and their potential for insect control, *Toxicon* 49 (2007) 423–435, <https://doi.org/10.1016/j.toxicon.2006.11.022>.
- [34] E. Chow, G.J.P. Singh, S.S. Gill, Binding and aggregation of the 25-kilodalton toxin of *Bacillus thuringiensis* subsp. *israelensis* to cell membranes and alteration by monoclonal antibodies and amino acid modifiers, *Appl. Environ. Microbiol.* 55 (1989) 2779–2788, <https://doi.org/10.1128/aem.55.11.2779-2788.1989>.
- [35] B. Promdonkoy, D.J. Ellar, Investigation of the pore-forming mechanism of a cytolytic delta-endotoxin from *Bacillus thuringiensis*, *Biochem. J.* 374 (2003) 255–259, <https://doi.org/10.1042/Bj20030437>.
- [36] B.H. Knowles, M.R. Blatt, M. Tester, J.M. Horsnell, J. Carroll, G. Menestrina, D.J. Ellar, A cytolytic  $\delta$ -endotoxin from *Bacillus thuringiensis* var. *israelensis* forms cation-selective channels in planar lipid bilayers, *FEBS Lett.* 244 (1989) 259–262, [https://doi.org/10.1016/0014-5793\(89\)80540-X](https://doi.org/10.1016/0014-5793(89)80540-X).
- [37] B.H. Knowles, D.J. Ellar, Colloid-osmotic lysis is a general feature of the mechanism of action of *Bacillus thuringiensis*  $\delta$ -endotoxins with different insect specificity, *Biochim. Biophys. Acta Gen. Subj.* 924 (1987) 509–518, [https://doi.org/10.1016/0304-4165\(87\)90167-X](https://doi.org/10.1016/0304-4165(87)90167-X).
- [38] E. Szabó, J. Murvai, P. Fábrián, F. Fábrián, M. Hollósi, J. Kajtár, Z. Buzás, M. Sajgó, S. Pongor, B. Asbóth, Is an amphiphilic region responsible for the haemolytic activity of *Bacillus thuringiensis* toxin? *Int. J. Pept. Protein Res.* 42 (1993) 527–532, <https://doi.org/10.1111/j.1399-3011.1993.tb00360.x>.
- [39] M.D. Peraro, F.G. van der Goot, Pore-forming toxins: ancient, but never really out of fashion, *Nat. Rev. Microbiol. advance on* (2015) 77–92, <https://doi.org/10.1038/nrmicro.2015.3>.
- [40] J. Du, B.H. Knowles, J. Li, D.J. Ellar, Biochemical characterization of *Bacillus thuringiensis* cytolytic toxins in association with a phospholipid bilayer, *Biochem. J.* 338 (1999) 185, <https://doi.org/10.1042/0264-6021:3380185>.
- [41] P. Butko, F. Huang, M. Pusztai-Carey, W.K. Surewicz, Membrane permeabilization induced by cytolytic delta-endotoxin CytA from *Bacillus thuringiensis* var. *israelensis*, *Biochemistry* 35 (1996) 11355–11360, <https://doi.org/10.1021/bi960970s>.
- [42] P. Butko, F. Huang, M. Pusztai-Carey, W.K. Surewicz, Interaction of the delta-endotoxin CytA from *Bacillus thuringiensis* var. *israelensis* with lipid membranes, *Biochemistry* 36 (1997) 12862–12868, <https://doi.org/10.1021/bi9702389>.
- [43] S. Tharad, B. Promdonkoy, J.L. Toca-Herrera, Protein-lipid interaction of cytolytic toxin Cyt2Aa2 on model lipid bilayers of erythrocyte cell membrane, *Toxins* 12 (2020), <https://doi.org/10.3390/toxins12040226>.
- [44] S. Tharad, J.L. Toca-Herrera, B. Promdonkoy, C. Krittanai, *Bacillus thuringiensis* Cyt2Aa2 toxin disrupts cell membranes by forming large protein aggregates, *Biosci. Rep.* 36 (2016), <https://doi.org/10.1042/BSR20160090>.
- [45] K.A. Brogden, Antimicrobial peptides: pore formers or metabolic inhibitors in bacteria? *Nat. Rev. Microbiol.* 3 (2005) 238–250, <https://doi.org/10.1038/nrmicro1098>.
- [46] G. Šolinc, T. Švigelj, N. Omersa, T. Snoj, K. Pirc, N. Žnidaršič, A. Yamaji-Hasegawa, T. Kobayashi, G. Anderluh, M. Podobnik, Pore-forming moss protein bryoporin is structurally and mechanically related to actinoporins from evolutionarily distant cnidarians, *J. Biol. Chem.* 298 (2022), <https://doi.org/10.1016/j.jbc.2022.102455/ATTACHMENT/C3F4F197-3234-49D1-8360-4415B10F482D/MMC1.DOCX>.
- [47] A. Punjani, J.L. Rubinstein, D.J. Fleet, M.A. Brubaker, CryoSPARC: algorithms for rapid unsupervised cryo-EM structure determination, *Nat. Methods* 14 (2017) 290–296, <https://doi.org/10.1038/nmeth.4169>.
- [48] E. deLello, W.K. Hanton, S.T. Bishoff, D.W. Misch, Histopathological effects of *Bacillus thuringiensis* on the midgut of tobacco hornworm larvae (*Manduca sexta*): low doses compared with fasting, *J. Invertebr. Pathol.* 43 (1984) 169–181, [https://doi.org/10.1016/0022-2011\(84\)90135-6](https://doi.org/10.1016/0022-2011(84)90135-6).
- [49] S. Tharad, J. Iturri, A. Moreno-Cencerrado, M. Mittendorfer, B. Promdonkoy, C. Krittanai, J.L. Toca-Herrera, Effect of the concentration of cytolytic protein Cyt2Aa2 on the binding mechanism on lipid bilayers studied by QCM-D and AFM, *Langmuir* 31 (2015) 10477–10483, <https://doi.org/10.1021/acs.langmuir.5b02849>.
- [50] S.C. Lin, Y.C. Lo, J.Y. Lin, Y.C. Liaw, Crystal structures and electron micrographs of fungal volvatoxin A2, *J. Mol. Biol.* 343 (2004) 477–491, <https://doi.org/10.1016/j.jmb.2004.08.045>.
- [51] S. Tharad, B. Promdonkoy, J.L. Toca-Herrera, Lipid phase influences the binding of *Bacillus thuringiensis* Cyt2Aa2 toxin on model lipid membranes, *Biochem. Biophys. Res. Commun.* 511 (2019) 409–415, <https://doi.org/10.1016/j.bbrc.2019.02.072>.
- [52] S. Tharad, Ö. Üzülmöz, B. Promdonkoy, J.L. Toca-Herrera, Cholesterol increases lipid binding rate and changes binding behavior of *Bacillus thuringiensis* cytolytic protein, *Int. J. Mol. Sci.* 19 (2018), <https://doi.org/10.3390/ijms19123819>.
- [53] J. Ferr, Jeroen Van Rie, *Biochemistry and genetics of insect resistance to Bacillus thuringiensis*, *Annu. Rev. Entomol.* 47 (2002) 501–533.